Ancillary Service to the Grid Using Intelligent Deferrable Loads

Sean Meyn, Prabir Barooah, Ana Bušić, Yue Chen, and Jordan Ehren

***Abstract*—Renewable energy sources such as wind and solar power have a high degree of unpredictability and time-variation, which makes balancing demand and supply challenging. One possible way to address this challenge is to harness the inherent flexibility in demand of many types of loads. Introduced in this paper is a technique for decentralized control for automated demand response that can be used by grid operators as ancillary service for maintaining demand-supply balance.**

A randomized control architecture is proposed, motivated by the need for decentralized decision making, and the need to avoid synchronization that can lead to large and detrimental spikes in demand. An aggregate model for a large number of loads is then developed by examining the mean field limit. A key innovation is an LTI (linear time-invariant) system approximation of the aggregate nonlinear model, with a scalar signal as the input and a measure of the aggregate demand as the output. This makes the approximation particularly convenient for control design at the grid level.

I. Introduction

Renewable energy penetration is rising rapidly throughout the world, and bringing with it high volatility in energy supply. Resources are needed to compensate for these large fluctuations in power. The federal energy regulatory commission (FERC) in conjunction with generation and utility companies are struggling to find resources, and finding ways to properly compensate for ancillary services that are badly needed by each *balancing authority* (BA) in the U.S. FERC orders 755 and 745 are examples of their attempts to provide incentives.

This paper concerns decentralized control of a large number of electric loads in a power grid. A particular load has a service it is intended to provide – clean dishes, hot water, or a clean pool. It is assumed that each load has some flexibility in energy consumption. This flexibility is harnessed to provide ancillary services to the power grid to help maintain stability, and to help offset any volatility in the grid because of line or generation outage, or because of the volatile nature of renewable energy. This is commonly called "demand response", but the meaning is slightly different here: The tuning of energy consumption is automated, and we want to ensure that the consumers do not suffer any degradation in the service offered by the loads.

We argue that most of the load in the U.S. is highly flexible, and this flexibility can be harnessed to provide ancillary service without central control, and without significant impact on the needs of consumers or industry.

Many utilities already employ demand response programs that use deferrable loads to reduce peak demand and manage emergency situations. Florida Power and Light (FPL), for example, has 780,000 customers enrolled in their *OnCall Savings Program* in which residential air conditioners, water heaters, and pool pumps systems are automatically controlled when needed [1]. Today, FPL uses this service only 3–4 times per year. While a valuable service to the grid, there is tremendous additional potential from these sources that today is virtually untapped.

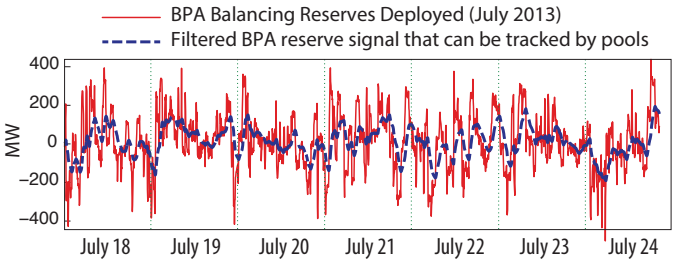

Fig. 1. *BPA Balancing Reserves Deployed* — Ancillary service needs at the BPA during one week in 2013. The maximum is approximately one-tenth of maximum load in this region.

Nearly all of America's ISOs/RTOs (Independent Systems Operators / Regional Transmission Organizations) also allow for demand side resources to participate in their regulation and spinning reserve markets, but as of the summer of 2013, only PJM (an RTO in the eastern U.S.) allows aggregation (with approval) [2].

Fig. 1 shows the *regulation signal* for a typical week within the Bonneville Power Authority (BPA) [3]. The variability seen in this figure is in part a consequence of variability of wind generation in this region. Generators in the region provide ancillary services in the form of power deviations: ramping their power output up and down to match this signal. Its role is analogous to the control signal in the feedback loop in a flight control system.

This regulation signal is *zero energy* on average, which means that some form of storage can be used as a substitute for ancillary service delivered by generators. We believe that flexible loads will be an inexpensive source of ancillary service – much cleaner and cheaper than generators or batteries.

To realize virtual storage from a flexible load it is necessary to consider constraints on the quality of service delivered by the load. In many cases these constraints can be interpreted in whole or in part by frequency bandwidth limitations. Each

This research is supported by the NSF grant CPS-0931416, CPS-093188, ECCS-0955023, the Department of Energy Awards DE-OE0000097 & DE-SC0003879, and the French National Research Agency grant ANR-12-MONU-0019. We acknowledge the help of Mark Rosenberg who offered many suggestions to improve the manuscript. We also send our thanks to the anonymous reviewers for their valuable and detailed feedback.

S.M., Y.C. and J.E. are with the Dept. ECE and P.B. is with the Dept. MAE at the University of Florida, Gainesville. A.B. is with Inria and the Computer Science Dept. of École Normale Supérieure, Paris, France.

class of loads can provide regulation only in a limited bandwidth, but the ensemble of all loads (perhaps in conjunction with generators, batteries, and other resources) can provide all of the ancillary service required by the BA.

In prior work it is shown how heating and ventilation systems in commercial buildings can provide service in a high frequency band, corresponding to periods ranging from under one minute to one hour [4]–[7]. As an example of implementation today, Alcoa provides 70 MW of frequency regulation service to the mid-continent ISO (MISO) by providing control over their aluminum smelting operation in Indiana. Growth of these resources in these wholesale markets has helped lower costs per megawatt-hour from 2009 to 2011 [2]. While recent analysis and implementation has focused on moderate frequency ancillary services [8], we believe that flexible manufacturing such as aluminum manufacturing can provide a large proportion of ancillary services at low frequencies (several hours to one day).

The focus of this paper is a large population of "on-off" loads. A control architecture is introduced to address privacy concerns and communication constraints, while allowing the power deviation of the collection of loads appear to the BA as a controllable resource. The information required at each load is minimal: In addition to its own internal state, it receives a regulation signal from the BA in real time, much as we can view BPA's regulation signal online today. The "intelligence" at the load amounts to decision making based on this information. These local control loops are designed so that the computational cost at each load is small.

Without a centralized architecture in which each load is managed individually by a balancing authority, it is essential to introduce randomization. This prevents synchronization, much like randomized congestion avoidance protocols in communication networks. First deployed nearly fifty years ago, ALOHA may be the first distributed communication protocol based on randomization [9]. *Random Early Detection* for congestion control was introduced in the highly influential paper [10]. The historical discussion in this paper points to significant research on randomized algorithms beginning in the early 1970s, following wide deployment of ALOHA. Randomized protocols are now standard practice in communication networks [9]. It is likely that randomized algorithms will become a standard feature of the power grid of the future.

To formulate a randomized control strategy, a Markovian Decision Process (MDP) model is proposed for an individual load. An aggregate model for a large number of loads is then obtained as a mean field limit.

A particular formulation of Todorov [11] is adopted because we can obtain an explicit solution, and because of available tools for analysis borrowed from the theory of large deviations. In particular, a key innovation in the present paper is an LTI (linear time-invariant) system approximation of the aggregate nonlinear model, which is possible through application of results from [12]. The scalar input in this linear model is a parameter that appears in the MDP cost function.

The LTI approximation is convenient for control design at the grid level: the input becomes the control signal that the BA will broadcast to all the loads, which adjusts a parameter in the randomized policy for the optimal MDP solution at each load.

In the second half of this paper we apply these general results to show how pool pumps can be harnessed to obtain ancillary service in a medium frequency band, corresponding to the dashed line in Fig. 1. This is the same BPA regulation signal, passed through a low pass filter.

Each residential pool has a pump that is the heart of its filtration system: it runs each day for a period of time ranging from 4 to 24 hours, and consumes over 1 kW of power when in operation. Consequently, the ability to control just half of the pool pumps in Florida or California amounts to over 500 MW of power [13]. Much of the control infrastructure is already in place [14]. Still, constraints and costs must be satisfied. These include run-times per day and per week, the cost of startup and shut down, as well as the total energy consumption. Moreover, there are privacy concerns and related communication constraints. Consequently, control algorithms must be distributed so that most of the required intelligence resides at individual pool pumps. In this paper we focus on constraints related to run-times per day, which is critical for keeping the water in the pool clean. Privacy and communication constraints will be addressed through the distributed control architecture.

The contributions of this paper are focused on control design at the load-level, and analysis of the aggregate. Due to space constraints, we do not include any analysis of the quality of service delivered to individual consumers. This topic is the subject of current research. Methods to estimate and eliminate risk to consumers are contained in the sequel [15].

A number of recent works have explored the potential for flexible loads for providing ancillary service. These include thermostatic loads to provide ancillary service in the time-scale of a few minutes (see [16]–[18] and refs. therein), electric vehicle charging [16], [19], [20] that can provide ancillary service in the time scale of a few hours, and our own recent work on harnessing ancillary service from commercial building HVAC systems on time scales from minutes to hours [4]–[7].

Mean-field games have been employed for analysis of aggregate loads in several recent papers [19], [20]. See [21]–[23] for more on general theory of mean-field technques.

The three papers [16], [24], [25] are most closely related to the present paper. Reference [24] proposes probabilistic algorithms for demand response, and presents analysis in a static setting. The more recent work [25] proposes a particular randomized algorithm for demand response in the context of voltage regulation on slow time-scales.

The paper [16] is closer to the control-theoretic setting of the present work. A mean field model is described as a bilinear state space model. This is converted to a linear model through division of the state. The control architecture consists of a centralized control signal computation based on state feedback, and the resulting input is broadcast to the devices.

The hierarchical architecture proposed in this paper is different from [16] because we introduce additional control at the load layer. We believe that some form of intelligence at each load is required so that it can can provide ancillary service to the grid, while maintaining quality of service constraints. We show that the aggregate behavior is well approximated by

a *single-input single-output, linear time-invariant* (SISO-LTI) system. Hence the control problem for the balancing authority can be addressed using classical control design methods. State estimation is not required — the information required at the BA is an estimate of the proportion of loads that are operating.

In the numerical example considered in this paper, this linear system is minimum-phase and stable, which is very helpful for control design.

The remainder of the paper is organized as follows. The control solution for a single pool is described in Section II, along with approximations of the optimal control solution based on general theory presented in the Appendix. The control of the aggregate collection of pools is considered in Section III. Conclusions and directions of future research are contained in Section IV.

II. Optimal control for a load and for the grid

A. Control architecture overview

We begin with a description of the control and information architecture. The components are illustrated in Fig. 2:

(i) There are N homogeneous loads that receive a common scalar command signal from the balancing authority, or BA, denoted $\boldsymbol{\zeta} = \{\zeta_t\}$ in the figure.

Randomization at each load is desirable to avoid synchronization of loads, and also to facilitate analysis of the aggregate system. It is assumed that each load evolves as a controlled Markov chain: the transition probability for each load is determined by its own state, and the BA signal $\boldsymbol{\zeta}$. The common dynamics are defined by a controlled transition matrix $\{P_\zeta : \zeta \in \mathbb{R}\}$. For the ith load, there is a state process $\boldsymbol{X}^i$ whose transition probability at time t is given by,

$$\mathsf{P}\{X^i_{t+1} = x^+ \mid X^i_t = x^-,\, \zeta_t = \zeta\} = P_\zeta(x^-, x^+) \quad (1)$$

where x^- and x^+ are possible state-values. The details of the model are described in Section II-B.

The complexity of this controller is modest. The collection of transition matrices $\{P_\zeta\}$ will be pre-computed, so that implementing (1) requires a simple 0/1 random number generator (a coin-flip). To reduce the amount of data stored at a load, the transition matrices can be approximated as explained in Section II-C.

(ii) The BA has measurements of the other two scalar signals shown in the figure: the normalized aggregate power consumption $\boldsymbol{y}$ and desired deviation in power consumption $\boldsymbol{r}$, also normalized via a division by N. When $\zeta_t = 0$ for all t, then the aggregate power consumption takes the value $\boldsymbol{y}^0$. This is the nominal power consumption of the collection of loads. The nominal behavior is referred to as "control-free" in this paper, indicating no interference by the BA on a load's operation. The goal of the BA is a problem of tracking the deviation from the nominal: achieve $y_t \approx y^0 + r_t$ for all t. This can be addressed using classical control techniques if the dynamics from $\boldsymbol{\zeta}$ to $\widetilde{\boldsymbol{y}} = \boldsymbol{y} - \boldsymbol{y}^0$ can be approximated by an LTI system.

The main contributions of this paper are based on the construction of the controlled transition matrix for an individual load, taking into account two potentially conflicting goals: (i) the BA desires overall dynamics from $\boldsymbol{\zeta}$ to $\boldsymbol{y}$ that facilitate tracking the reference signal $\boldsymbol{r}$, and (ii) each load requires good quality of service. In the case of a pool, the water must be kept clean, and the electricity bill must not increase.

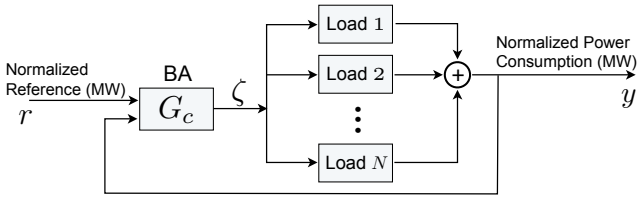

Fig. 2. The control architecture: command $\boldsymbol{\zeta}$ is computed at a BA, and transmitted to each pool pump. The control decision at a load is binary (turn on/off), and is based only on its own state and the signal $\boldsymbol{\zeta}$.

The main results of this paper are based on a particular approach to the design of the parameterized family of transition matrices. The structure of the family of controlled transition matrices leads to the LTI approximation of the input-output dynamics from $\boldsymbol{\zeta}$ to $\widetilde{\boldsymbol{y}}$ that is presented in Proposition 2.4.

Example: In the second half of the paper we focus on a particular example in which each load is a residential pool pump.

The true nominal behavior would be deterministic – most consumers set the pump to run a fixed number of hours each day. Regardless, for the purposes of design and analysis it is useful to introduce some randomness in the nominal model P_0. The values of $P_0(x, y)$ will be chosen to be nearly 0 or 1 for most $x, y \in \mathsf{X}$ to model nearly deterministic behavior of a pool pump in the control-free case. The state space is taken to be the finite set,

$$\mathsf{X} = \{(m, i) : m \in \{\oplus, \ominus\},\ i \in \{1, \ldots, \mathcal{I}\}\} \quad (2)$$

where $\mathcal{I} > 1$ is an integer.

If $X_t = (\ominus, i)$, this indicates that the pool-pump is off at sampling time t and has remained off for the previous i time units (including the current time t), and $X_t = (\oplus, i)$ represents the alternative that the pool-pump has been operating continuously for exactly i time units. A state-transition diagram is shown in Fig. 3.

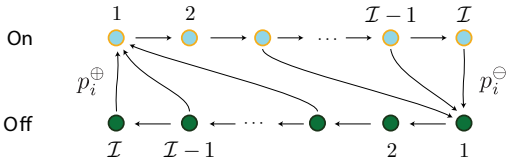

Fig. 3. State transition diagram for the pool-pump model.

In this example it is found that the LTI approximation is minimum phase, and that a simple PI (proportional-integral) controller can be effectively used for the control transfer function G_c shown in Fig. 2. □

B. Design

In this subsection we describe a procedure to construct the controlled transition matrix appearing in (1). The controlled

Markov chain evolves on a finite state space, denoted $\mathsf{X} = \{x^1, \dots, x^d\}$. The construction is based on an optimal control problem for an individual load, taking into account the needs of the load and the grid.

It is assumed that a transition matrix P_0 is given that models "control free" behavior of the Markov chain, and a utility function $\mathcal{U}\colon \mathsf{X} \to \mathbb{R}$ is used to model the needs of the grid. The optimal control problem will balance average utility and the cost of deviation.

Since we focus on a single load, in this subsection the index i in (1) is dropped, and we denote by $\boldsymbol{X} = (X_0, X_1, \dots)$ the stochastic process evolving on X that models this load.

Consider first a finite-time-horizon optimization problem: for a given terminal time T, let p_0 denote the probability mass function on strings of length T:

$$p_0(x_1, \dots, x_T) = \prod_{i=0}^{T-1} P_0(x_i, x_{i+1}) \,,$$

where $x_0 \in \mathsf{X}$ is assumed to be given. A fixed scalar $\zeta \in \mathbb{R}$ is interpreted as a *weighting parameter* in the following definition of *total welfare*. For any probability mass function p, this is defined as the weighted difference,

$$\mathcal{W}_T(p) = \zeta \mathsf{E}_p\Big[\sum_{t=1}^{T} \mathcal{U}(X_t)\Big] - D(p \| p_0) \tag{3}$$

where the expectation is with respect to p, and D denotes relative entropy:

$$D(p\|p_0) := \sum_{x_1,\dots,x_T} \log\Big(\frac{p(x_1,\dots,x_T)}{p_0(x_1,\dots,x_T)}\Big) p(x_1,\dots,x_T)$$

The finite horizon problem admits a unique solution denoted p_T^*, whose form is described in Proposition 2.1 below.

The infinite-horizon mean welfare is denoted,

$$\eta_\zeta^* = \lim_{T\to\infty} \frac{1}{T} \mathcal{W}_T(p_T^*) \tag{4}$$

We show in Proposition 2.2 that the infinite-horizon performance η_ζ^* can be obtained from a Markovian model whose transition law is denoted $\check{P}_\zeta$[1]. This is used to define the randomized policy described in Section II-A.

The two terms in the welfare function (3) represent the two conflicting goals: to provide service to the grid and to reduce deviation of the load's behavior from the nominal. If the controlled probability p is chosen to be different from p_0, it potentially reduces the quality of service to the consumer, which is modeled by the term "$-D(p\|p_0)$".

Consider the case in which $\mathcal{U}(X_t)$ is equal to the power consumption of the load. If the grid operator requires lower power demand than the nominal value, this goal is modeled through the first term in (3) whenever the parameter ζ is positive.

We next characterize the optimizer of the total welfare.

[1]The notation is introduced to distinguish these from an arbitrary collection of transition matrices; this notation is consistent with the 'twisted transition matrix' considered in [12].

Proposition 2.1: The probability mass function p_T^* that maximizes the total welfare (3) is the *twisted distribution*,

$$p_T^*(x_1^T) = \exp\Big(\zeta \sum_{t=1}^{T} \mathcal{U}(x_t) - \Lambda_T(\zeta)\Big) p_0(x_1^T) \tag{5}$$

where $x_1^T = (x_1, \dots, x_T)$ and

$$\Lambda_T(\zeta) = \log\Big\{\mathsf{E}\Big[\exp\Big(\zeta \sum_{t=1}^{T} \mathcal{U}(X_t)\Big)\Big]\Big\}\,, \tag{6}$$

where the expectation is with respect to p_0. Moreover, $\mathcal{W}_T(p_T^*) = \Lambda_T(\zeta)$ is the optimal value. □

Proof: Optimality of p_T^* follows from convex duality between the log moment generating function and relative entropy – [26, Proposition II.1] and [27, Lemma 2.39]. The formula (6) follows from the fact that p_T^* sums to unity, so that $\Lambda_T(\zeta)$ can be interpreted as a normalizing constant.

The identity $\mathcal{W}_T(p_T^*) = \Lambda_T(\zeta)$ follows from the definitions of $\mathcal{W}_T$ and p_T^*. □

The probability mass function p_T^* defines a Markov chain on the time interval $\{0, 1, \dots, T\}$ (with $X_0 = x_0$ given), but it is not necessarily time-homogeneous. In the infinite horizon case, we would like to find a distribution p^* on infinite sequences that attains the optimal average welfare (4).

A solution to the infinite horizon problem is given by a time-homogenous Markov chain whose transition matrix is obtained following the solution of an eigenvector problem, based on the $d \times d$ matrix,

$$\widehat{P}(x,y) = \exp(\zeta \mathcal{U}(x)) P_0(x,y)\,, \qquad x, y \in \mathsf{X}\,. \tag{7}$$

Let $\lambda > 0$ denote the Perron-Frobenious eigenvalue, and v the eigenvector with non-negative entries satisfying,

$$\widehat{P} v = \lambda v \tag{8}$$

We introduce subscripts, e.g. $\lambda = \lambda_\zeta$, when the value of the parameter must be emphasized.

Representations for λ and v are contained in Section II-C. The proof of Proposition 2.2 is given in Section A of the Appendix.

Proposition 2.2: If P_0 is irreducible, an optimizing p^* that achieves (4) is defined by a time-homogeneous Markov chain whose transition probability is defined by,

$$\check{P}_\zeta(x,y) = \frac{1}{\lambda} \frac{1}{v(x)} \widehat{P}(x,y) v(y)\,, \qquad x, y \in \mathsf{X}, \tag{9}$$

where $\widehat{P}$ is the scaled transition matrix (7). The eigenvector v has positive entries and is unique up to constant multiples. The eigenvalue λ is also positive.

In addition, the following bounds hold for each T. Let $\check{p}_T$ denote the probability on X^T induced by $\check{P}_\zeta$, with initial condition x_0 given. Denote $\Lambda = \log(\lambda)$, and

$$h^*(x) = \log(v(x)), \qquad x \in \mathsf{X}. \tag{10}$$

Then,

$$\begin{aligned} 0 \le \mathcal{W}_T(p_T^*) - \mathcal{W}_T(\check{p}_T) &\le 2\|h^*\|_{\text{sp}} \\ |T\Lambda - \mathcal{W}_T(p_T^*)| &\le \|h^*\|_{\text{sp}} \end{aligned} \tag{11}$$

where the span norm is defined by $\|h^*\|_{\text{sp}} = \max h^* - \min h^*$. Consequently, the Markov model achieves the optimal average welfare (4) with $\eta_\zeta^* = \Lambda$. □

The eigenvector problem (8) appears in multiplicative ergodic theory [12], and also in Todorov's analysis [11]. It is shown in [11] that the *relative value function* appearing in the average cost optimality equations is the logarithm of the eigenvector, which is denoted h^* in (10). See also the derivation in [28] for a variant of this model.

Second order Taylor series approximations for v and η^* near $\zeta \approx 0$ can be found by borrowing tools from large-deviations theory. Some of these approximation results are new, and are collected together in the next section and in the Appendix.

C. Approximations

Approximations will be needed for analysis when we extend the model to allow ζ to change with time. Throughout the paper we take for granted that λ_ζ and h_ζ are differentiable in ζ. Justification is based on the spectral analysis in Section 3.2 of [12].

A solution to the eigenvector problem (8) can be represented through a regenerative formula. Let $\boldsymbol{\alpha} \in \mathsf{X}$ be some fixed state that is reachable from each initial condition of the chain, under the transition law P_0. That is, the chain is assumed to be $\boldsymbol{\alpha}$-irreducible [29]. Since the state space is assumed to be finite, it follows that there is a unique invariant probability mass function π_0 for P_0. The first return time is denoted,

$$\tau = \min\{t \ge 1 : X_t = \boldsymbol{\alpha}\}\,.$$

Recall that the infinite horizon optimal welfare is given by $\eta_\zeta^* = \log(\lambda)$. From the theory of positive matrices [12], [30], [31], it follows that it is the unique solution to,

$$1 = \mathsf{E}_\alpha\Big[\exp\Big(\sum_{t=0}^{\tau-1}[\zeta\mathcal{U}(X_t) - \eta_\zeta^*]\Big)\Big] \tag{12}$$

where the subscript indicates that the initial condition is $X(0) = \boldsymbol{\alpha}$. Moreover, for each $x \in \mathsf{X}$, the value of $v(x)$ is obtained as the expected sum, with initial condition $X(0) = x$:

$$v(x) = \mathsf{E}_x\Big[\exp\Big(\sum_{t=0}^{\tau-1}[\zeta\mathcal{U}(X_t) - \eta_\zeta^*]\Big)\Big] \tag{13}$$

These expectations are each with respect to the nominal transition law P_0.

A Taylor-series approximation of η_ζ^* is based on two parameters, defined with respect to the nominal model P_0 with invariant probability mass function π_0. The first-order coefficient is the the steady-state mean:

$$\eta_0 = \sum_x \pi_0(x)\mathcal{U}(x) \tag{14}$$

The second-order coefficient is based on the *asymptotic variance* of $\mathcal{U}$ for the nominal model (the variance appearing in the Central Limit Theorem (CLT) for the nominal model). For this finite state space model this has two similar representations,

$$\begin{aligned}\kappa^2 &= \lim_{T\to\infty}\frac{1}{T}\mathsf{E}\Big[\Big(\sum_{t=0}^{T-1}\widetilde{\mathcal{U}}(X_t)\Big)^2\Big] \\ &= \pi_0(\boldsymbol{\alpha})\mathsf{E}_\alpha\Big[\Big(\sum_{t=0}^{\tau-1}\widetilde{\mathcal{U}}(X_t)\Big)^2\Big]\end{aligned} \tag{15}$$

where

$$\widetilde{\mathcal{U}} = \mathcal{U} - \eta_0. \tag{16}$$

See [29, Theorem 17.0.1] for the CLT, and eqn. (17.13) of [29] for the second representation above.

Similarly, the following functions of x are used to define a second order Taylor series approximation for h_ζ^*. The first-order term is the solution to *Poisson's equation* for P_0,

$$H(x) = \mathsf{E}_x\Big[\sum_{t=0}^{\tau-1}\widetilde{\mathcal{U}}(X_t)\Big] \tag{17}$$

The asymptotic variance can be expressed in terms of Poisson's equation [29], [32]:

$$\kappa^2 = \sum_x \pi_0(x)\big(2\widetilde{\mathcal{U}}(x)H(x) - \widetilde{\mathcal{U}}(x)^2\big)$$

The second-order term in an approximation of v is another variance,

$$\mathcal{S}(x) = \mathsf{E}_x\Big[\Big(\sum_{t=0}^{\tau-1}\widetilde{\mathcal{U}}(X_t)\Big)^2\Big] - \big(H(x)\big)^2\,, \quad x \in \mathsf{X}. \tag{18}$$

Proposition 2.3: The following hold for the finite state space model in which P_0 is irreducible:

(i) The optimal average welfare η_ζ^* is convex as a function of ζ, and admits the Taylor series expansion,

$$\eta_\zeta^* = \eta_0\zeta + \tfrac{1}{2}\kappa^2\zeta^2 + O(\zeta^3) \tag{19}$$

(ii) The mean of $\mathcal{U}$ under the the invariant probability mass function $\check{\pi}_\zeta$ for $\check{P}_\zeta$ is given by,

$$\sum_x \check{\pi}_\zeta(x)\mathcal{U}(x) = \frac{d}{d\zeta}\eta_\zeta^* \tag{20}$$

This admits the first-order Taylor series approximation

$$\frac{d}{d\zeta}\eta_\zeta^* = \eta_0 + \kappa^2\zeta + O(\zeta^2) \tag{21}$$

(iii) The relative value function (10) admits the second-order Taylor series approximation,

$$h_\zeta^*(x) = \zeta H(x) + \tfrac{1}{2}\zeta^2\mathcal{S}(x) + O(\zeta^3) \tag{22}$$

□

Proof: Equations (19)—(21) follow from the fact that $\eta_\zeta^* = \log(\lambda)$ can be expressed as a cumulative log-moment generating function [12, Prop. 4.9].

Convexity follows from the fact that η_ζ^* is the maximum of linear functions of ζ (following the linear-program formulation of the ACOE [33]).

The approximation (22) follows from the the representation (13) for v, and the definition $h_\zeta^* = \log(v)$ (see (10)). □

The representations in this subsection are useful for analysis, but not for computation. Methods to compute H and $\mathcal{S}$ are contained in Section B2 of the Appendix.

D. Aggregate load model

Consider N loads operating under the distributed control architecture surveyed in Section II-A. The state of the ith load is denoted X_t^i.

The previous subsections focused on design of the local transition matrices $\{\check{P}_\zeta : \zeta \in \mathbb{R}\}$. We now consider the control problem faced by the BA: how to choose the sequence $\boldsymbol{\zeta} = (\zeta_0, \zeta_1, \dots)$ to provide service to the grid, while maintaining quality of service constraints for the loads. It is assumed that the BA has measurements of a regulation signal $\boldsymbol{r}$, and the average utility $\boldsymbol{y}$: At time t this is given by

$$y_t = \frac{1}{N}\sum_{i=1}^{N} \mathcal{U}(X_t^i). \tag{23}$$

Control design is based on a model of the input-output system, whose input is $\boldsymbol{\zeta}$ and output $\boldsymbol{y}$. The model is obtained in two steps.

In step 1 the existence of a mean-field limit is assumed (to be justified in Theorem 2.5): let $N \to \infty$ to obtain

$$\lim_{N\to\infty} \frac{1}{N}\sum_{i=1}^{N} \mathbb{I}\{X_t^i = x\} = \mu_t(x)\,, \quad x \in \mathsf{X}. \tag{24}$$

For a given initial distribution μ_0 on X, the distribution μ_t is defined by $\mu_t(x_t) =$

$$\sum_{x_i \in \mathsf{X}} \mu_0(x_0)\check{P}_{\zeta_0}(x_0, x_1)\check{P}_{\zeta_1}(x_1, x_2)\cdots\check{P}_{\zeta_{t-1}}(x_{t-1}, x_t) \tag{25}$$

where x_t is an arbitrary state in X, and the sum is over all intermediate states. We view $\{\mu_t\}$ as a state process that is under our control through $\boldsymbol{\zeta}$.

Step 2 is based on the Taylor series approximations surveyed in the previous section to approximate this nonlinear system by a linear state space model with d-dimensional state $\boldsymbol{\Phi}$ and output $\boldsymbol{\gamma}$. It is defined so that for any time t, and any i,

$$\begin{aligned}\mu_t(x^i) &= \pi_0(x^i) + \Phi_t(i) + O(\|\boldsymbol{\zeta}\|^2)\\ \gamma_t &= \tilde{y}_t + O(\|\boldsymbol{\zeta}\|^2)\end{aligned}$$

where $\tilde{y}_t = y_t - y^0$, with $y^0 = \sum_x \pi_0(x)\mathcal{U}(x)$, and $O(\|\boldsymbol{\zeta}\|^2) = O(\zeta_0^2 + \cdots + \zeta_t^2)$.

Proposition 2.4: Consider the nonlinear state space model whose state evolution is $\mu_{t+1} = \mu_t\check{P}_{\zeta_t}$, and output is $y_t = \sum_x \mu_t(x)\mathcal{U}(x)$. Its unique equilibrium with $\boldsymbol{\zeta} \equiv 0$ is $\mu_t \equiv \pi_0$ and $y_t \equiv y^0 := \sum_x \pi_0(x)\mathcal{U}(x)$. Its linearization around this equilibrium is defined by the state space model,

$$\begin{aligned}\Phi_{t+1} &= A\Phi_t + B\zeta_t\\ \gamma_t &= C\Phi_t\end{aligned} \tag{26}$$

with initial condition $\Phi_0(i) = \mu_0(x^i) - \pi_0(x^i)$, $1 \le i \le d$. In this model $A = P_0^{\intercal}$, C is a row vector of dimension $d = |\mathsf{X}|$ with $C_i = \mathcal{U}(x^i)$ for each i, and B is a d-dimensional column vector with entries $B_j = \sum_x \pi_0(x)\mathcal{E}(x, x^j)$, where

$$\mathcal{E}(x^i, x^j) = \Big[\widetilde{\mathcal{U}}(x^i) + H(x^j) - H(x^i)\Big]P_0(x^i, x^j) \tag{27}$$

for each $x^i, x^j \in \mathsf{X}$. The matrix $\mathcal{E}$ is equal to the derivative,

$$\mathcal{E} = \frac{d}{d\zeta}\check{P}_\zeta\Big|_{\zeta=0}$$

Proof: The formulae for A and C follow from the fact that the system is linear in the state.

To establish the formula for B based on (27) we begin with a representation that follows from (9),

$$\check{P}_\zeta(x^i, x^j) = e^{\zeta\mathcal{U}(x^i) - \eta_\zeta^* - h_\zeta^*(x^i)}P_0(x^i, x^j)e^{h_\zeta^*(x^j)}$$

where η_ζ^* is defined in (4), and h_ζ^* is defined in (10). Based on the first order approximation of h_ζ^* in Proposition 2.3 we obtain,

$$\check{P}_\zeta(x^i, x^j) = e^{\zeta[-H(x^i) + \widetilde{\mathcal{U}}(x^i)]}P_0(x^i, x^j)e^{\zeta H(x^j)} + O(\zeta^2)$$

where H is a solution to Poisson's equation (with forcing function $\mathcal{U}$) for the nominal model (see (17)), and $\widetilde{\mathcal{U}}$ is defined in (16). Using a first order Taylor series for the exponential then gives,

$$\begin{aligned}\check{P}_\zeta(x^i, x^j) &= [1 - \zeta(H(x^i) - \widetilde{\mathcal{U}}(x^i))]P_0(x^i, x^j)[1 + \zeta H(x^j)]\\ &\qquad + O(\zeta^2)\\ &= P_0(x^i, x^j) + \zeta\mathcal{E}(x^i, x^j) + O(\zeta^2)\end{aligned}$$

If $\mu = \pi_0 + O(\zeta)$ and ζ is small, then we can approximate,

$$\mu\check{P}_\zeta = \mu P_0 + \zeta B^{\intercal} + O(\zeta^2)\,,$$

where B is the vector with entries $B_j = \sum_x \pi_0(x)\mathcal{E}(x, x^j)$. □

Next we justify the mean-field model (24).

For the purpose of analysis we lift the state space from the d-element set $\mathsf{X} = \{x^1, \cdots, x^d\}$, to the space of probability mass functions on X. This is denoted S since it can be identified as the d-dimensional unit simplex.

For the i^{th} load at time t, the element $\pi_t^i \in \mathsf{S}$ is the degenerate distribution whose mass is concentrated at x if $X_t^i = x$. The average over N, denoted $\mu_t^N \in \mathsf{S}$, is the empirical distribution,

$$\mu_t^N(x) = \frac{1}{N}\sum_{i=1}^{N}\pi_t^i(x) = \frac{1}{N}\sum_{i=1}^{N}\mathbb{I}\{X_t^i = x\}\,, \quad x \in \mathsf{X}$$

In the proof of convergence it is assumed that $\boldsymbol{\zeta}^N$ is obtained using state feedback of the form,

$$\zeta_t^N = \phi_t(\mu_0^N, \dots, \mu_t^N)$$

where $\phi_t \colon \mathsf{S}^{t+1} \to \mathbb{R}$ is continuous for each t, and does not depend upon N. The following result establishes convergence.

Theorem 2.5: Suppose $\mu_0^N \to \mu_0$ as $N \to \infty$. Then for each t,

$$\lim_{N\to\infty} \mu_t^N = \mu_t, \qquad \textit{with probability one,} \tag{28}$$

where the right hand side denotes the probability mass function (25), in which

$$\zeta_t = \phi_t(\mu_0, \dots, \mu_t), \qquad t \ge 0.$$

□

While Theorem 2.5 and other results in this section are based on the particular transition matrices constructed in

Proposition 2.2, the main results hold in far greater generality. In particular, Theorem 2.5 only requires continuity in ζ of a family of the transition matrices $\{P_\zeta : \zeta \in \mathbb{R}\}$.

The proof of this result is given at the end of this subsection, and is based on a version of the Law of Large Numbers for martingales.

Let $\{M_{N,k}, 1 \le k \le N\}$ denote a (vector-valued) martingale array: This is a vector-valued sequence satisfying $\mathsf{E}[M_{N,k}|M_{N,1}, \cdots M_{N,k-1}] = M_{N,k-1}$ for each N and $1 < k \le N$. We denote $M_N = M_{N,N}$.

Proposition 2.6: Suppose that $\{M_{N,k}\}$ is a martingale array, and suppose that it has bounded increments, i.e., for some $c_m < \infty$,

$$\|M_{N,k+1} - M_{N,k}\| \le c_m \qquad \text{for all } k \text{ and } N$$

Then the Law of Large Numbers holds:

$$\lim_{N\to\infty} \frac{1}{N}\|M_N\| = 0, \qquad \textit{with probability one.}$$

□

Proof: The Hoeffding-Azuma inequality [34] gives the following bound:

$$\mathsf{P}\{N^{-1}|M_N^i| \ge t\} \le 2\exp(-[Nt]^2/[2Nc_m^2])$$

where M_N^i is the ith entry of the vector M_N. The right hand is summable, so the result follows from the Borel-Cantelli Lemma. □

Proposition 2.6 is applied to show that the sequence of empirical distribution μ_t^N can be approximated by the mean-field model perturbed by a disturbance that vanishes as $N \to \infty$:

Lemma 2.7: The empirical distributions $\{\mu_t^N : t \ge 0\}$ obey the recursion

$$\mu_{t+1}^N = \mu_t^N \check{P}_{\zeta_t^N} + W_{t+1}^N, \tag{29}$$

in which, $W_{t+1}^N = \frac{1}{N}\sum_{i=1}^N \Delta_{t+1}^i$ for a family of vector random variables $\{\Delta_{t+1}^i\}$.

On denoting $M_{N,k} = \sum_{i=1}^k \Delta_t^i$ we have,

(i) $\{M_{N,k} : 1 \le k \le N\}$ is a martingale array.

(ii) There exists c_m such that $\|M_{N,k} - M_{N,k-1}\| \le c_m$ for all N and all k such that $1 < k \le N$.

Proof of Lemma 2.7: to establish (29) we first establish a similar expression for $\{\pi_t^i\}$.

For each i, the sequence of degenerate distributions $\{\pi_t^i\}$ evolve according to a random linear system,

$$\pi_{t+1}^i = \pi_t^i G_{t+1}^i \tag{30}$$

in which π_t^i is interpreted as a d-dimensional row vector, and G_{t+1}^i is a $d \times d$ matrix with entries 0 or 1 only, and $\sum_l G_{t+1}^i(x^j, x^l) = 1$ for all j. The matrix G_{t+1}^i is conditionally independent of $\{\pi_0^i, \cdots, \pi_t^i\}$, given ζ_t^N, with

$$\mathsf{E}[G_{t+1}^i|\pi_0^i, \cdots, \pi_t^i, \zeta_t^N] = \check{P}_{\zeta_t^N}. \tag{31}$$

Dependency of π_t^i, G_t^i on N is suppressed, but we must distinguish ζ_t^N from its limit ζ_t.

The random linear system (30) can thus be described as a linear system driven by "white noise":

$$\pi_{t+1}^i = \pi_t^i \check{P}_{\zeta_t^N} + \Delta_{t+1}^i \tag{32}$$

where, $\{\Delta_{t+1}^i = \pi_t^i(G_{t+1}^i - \check{P}_{\zeta_t^N}) : t \ge 1\}$, which establishes (29).

The following representation will clarify the remaining analysis: for some function Ξ with domain $\mathbb{R} \times [0,1]$, and range equal to the set of $d \times d$ matrices,

$$G_t^i = \Xi(\zeta_{t-1}^N, \xi_t^i), \tag{33}$$

where $\{\xi_t^i : t \ge 1,\ i \ge 1\}$ are i.i.d. on $[0,1]$. For $1 \le i < N$ and fixed t, we define two σ-algebras:

$$\mathcal{F}_i = \sigma\{\Delta_t^k, k \le i\}$$
$$\mathcal{H}_i = \sigma\{\pi_{t-1}^{k+1}, \zeta_{t-1}^N, \Delta_t^k, k \le i\}$$

Under (33) we have the extension of (31), that $\mathsf{E}[G_t^{i+1} \mid \mathcal{H}_i] = \check{P}_{\zeta_{t-1}^N}$. Moreover, by construction the random variable π_{t-1}^{i+1} is $\mathcal{H}_i$-measurable. Therefore,

$$\mathsf{E}[\Delta_t^{i+1} \mid \mathcal{H}_i] = \mathsf{E}[\pi_{t-1}^{i+1}(G_t^{i+1} - \check{P}_{\zeta_{t-1}^N}) \mid \mathcal{H}_i] = 0$$

The construction $\mathcal{F}_i \subset \mathcal{H}_i$ then gives (i),

$$\mathsf{E}[\Delta_t^{i+1} \mid \mathcal{F}_i] = \mathsf{E}[\mathsf{E}[\Delta_t^{i+1} \mid \mathcal{H}_i] \mid \mathcal{F}_i] = 0$$

From the definition of Δ_t^i below equation (32), it follows that $\{\|\Delta_t^i\|\}$ admits a uniform bound. Consequently, $\|M_{N,k} - M_{N,k-1}\| = \|\Delta_t^k\|$ is bounded, which is (ii). □

Proof of Theorem 2.5: Denote, for $T \ge 0$, the deviation $\tilde{\mu}_T^N = \mu_T^N - \mu_T$. We prove by induction on T that $\tilde{\mu}_T^N \to 0$ as $N \to \infty$. This holds by assumption when $T = 0$.

Suppose now that (28) holds for $t \le T$. By continuity of ϕ_t, it follows that $\zeta_t^N \to \zeta_t$ as $N \to \infty$. We also have by Lemma 2.7,

$$\tilde{\mu}_{T+1}^N = \tilde{\mu}_T^N \check{P}_{\zeta_T} + \mu_T^N(\check{P}_{\zeta_T^N} - \check{P}_{\zeta_T}) + W_{T+1}^N$$

Lemma 2.7 and Proposition 2.6 imply that $W_{T+1}^N \to 0$ as $N \to \infty$. Continuity of $\check{P}_\zeta$ then implies that

$$\lim_{N\to\infty} \tilde{\mu}_{T+1}^N = 0$$

□

III. Controlling a large number of pools

For the remainder of the paper we apply the results of the previous section to the control of a large population of residential pools. The nominal transition matrix P_0 is defined by the probabilities of turning the pump on or off, as illustrated in the state transition diagram Fig. 3. In many of the numerical results described below a symmetric model was chosen for P_0 in which the nominal cleaning cycle is equal to 12 hours, and $p^\oplus(i) = p^\ominus(i)$, where

$$p^\oplus(i) := \mathsf{P}\{\text{pump switches on} \,|\, \text{it has been off } i \text{ hours}\}$$
$$p^\ominus(i) := \mathsf{P}\{\text{pump switches off} \,|\, \text{it has been on } i \text{ hours}\}$$

The utility function $\mathcal{U}$ is chosen as the indicator function that the pool pump is operating:

$$\mathcal{U}(x) = \sum_{i=1}^{\mathcal{I}} \mathbb{I}\{x = (\oplus, i)\} \tag{34}$$

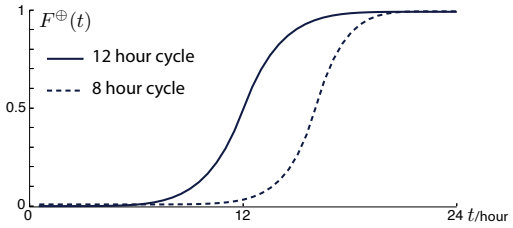

Fig. 4. Control free behavior of a pool with a 12-hour cleaning cycle (solid), and 8-hour cycle (dashed).

It remains to give numerical values for $p^{\oplus}(i)$ and $p^{\ominus}(i)$, $1 \le i \le \mathcal{I}$. It is convenient to first consider a model in *continuous time*.

Let $\tau_{\oplus}$ denote a random variable whose distribution models the typical time-interval that the pool is off in the nominal model. Its cumulative distribution function (CDF) is denoted,

$$F^{\oplus}(t) = \mathsf{P}\{\tau_{\oplus} \le t\} \qquad 0 \le t \le \mathcal{T},$$

where $\mathcal{T} = 24$ hours. On denoting the complimentary CDF by $\overline{F}^{\oplus}(\cdot) = 1 - F^{\oplus}(\cdot)$, the mean of this random variable is expressed

$$\mathsf{E}[\tau_{\oplus}] = \int_0^{\mathcal{T}} \overline{F}^{\oplus}(t)\, dt$$

If, say, we choose a sampling time $T_s = 30$ minutes then we will quantize $\tau_{\oplus}$,

$$\tau_{\oplus}^{\Delta} = T_s \lceil \tau_{\oplus}/T_s \rceil$$

The probability that the pool turns on at time $t = iT_s$ is given by,

$$\begin{aligned} p^{\oplus}(i) &= \mathsf{P}\{\tau_{\oplus}^{\Delta} = iT_s \mid \tau_{\oplus}^{\Delta} > (i-1)T_s\} \\ &= \mathsf{P}\{\tau_{\oplus} \le iT_s \mid \tau_{\oplus} > (i-1)T_s\} \\ &= \frac{1}{\overline{F}^{\oplus}((i-1)T_s)} \Big(F^{\oplus}(iT_s) - F^{\oplus}((i-1)T_s) \Big) \end{aligned} \tag{35}$$

In the symmetric model, the CDF was constrained to the following parametric family: For fixed $\gamma > 1$,

$$F_s^{\oplus}(t) = F_s^{\ominus}(t) = \begin{cases} 2^{\gamma-1} t^{\gamma} & 0 \le t \le 1/2 \\ 1 - 2^{\gamma-1}(1-t)^{\gamma} & 1/2 \le t \le 1 \end{cases} \tag{36}$$

Fig. 4 shows a plot of this CDF with $\gamma = 6$

To go beyond the symmetric model, a parameter α is introduced to represent the fraction of the day that the pool is operating. The two CDFs are modified as follows,

$$F^{\oplus}(t) = F_s^{\oplus}(t^{\delta_+}), \qquad F^{\ominus}(t) = F_s^{\oplus}(x^{\delta_-}) \tag{37}$$

where δ_+ is chosen so that $0.5^{\delta_+} = 1-\alpha$, or $\delta_+ = -\log_2(1-\alpha)$, and similarly $\delta_- = -\log_2(\alpha)$. Hence the median of $\tau_{\oplus}$ is equal to $(1-\alpha)\mathcal{T}$, and the median of $\tau_{\ominus}$ is equal to $\alpha\mathcal{T}$.

As $\gamma \to \infty$, the functions in (37) will converge to step functions corresponding to a deterministic cleaning period of $\alpha \times 24$ hours. We find numerically that the mean approximates the median when $\gamma \ge 3$ and $\alpha \in [1/3, 1/2]$. The CDF $F^{\oplus}$ with $\alpha = 1/3$ and $\gamma = 6$ is represented as the dashed line in Fig. 4.

A. Approximations

The steady-state probability that a pool-pump is in operation is given by

$$\check{P}_{\zeta}\{\text{pool-pump is on}\} = \sum_x \check{\pi}_{\zeta}(x)\mathcal{U}(x)$$

A linear approximation is obtained in Proposition 2.3 (ii):

$$\check{P}_{\zeta}\{\text{pool-pump is on}\} = \eta_0 + \kappa^2\zeta + O(\zeta^2) \tag{38}$$

A comparison of the true probability and its affine approximation is shown in Fig. 5 for the symmetric model, in which $\eta_0 = 1/2$. The approximation is very tight for $|\zeta| \le 2$. For larger values of ζ the true steady-state probability saturates.

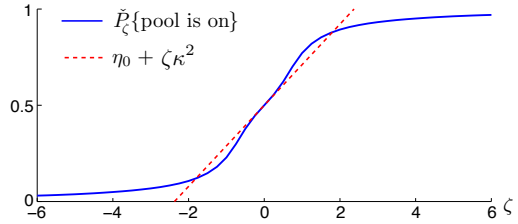

Fig. 5. Approximation of the steady-state probability that a pool-pump is operating under $\check{P}_{\zeta}$.

For each ζ, the controlled model $\check{P}_{\zeta}$ has the same form as P_0, with transformed probability vectors $\check{p}_{\zeta}^{\oplus}$ and $\check{p}_{\zeta}^{\ominus}$. Fig. 6 contains plots of the transformed vector $\check{p}_{\zeta}^{\oplus}$ for values $\zeta = 0, \pm 2, \pm 4$, and also the corresponding discrete CDFs. The plots of $\check{p}_{\zeta}^{\ominus}$ are obtained through symmetry.

The approximation of the average welfare established in Proposition 2.3 is,

$$\eta_{\zeta}^* = \eta_0\zeta + \tfrac{1}{2}\kappa^2\zeta^2 + O(\zeta^3) \tag{39}$$

Shown in Fig. 7 is a comparison of η_{ζ}^* with linear and quadratic approximations based on (39).

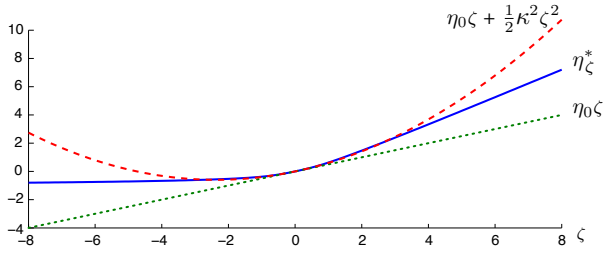

Fig. 7. The optimal average welfare η_{ζ}^* and its quadratic approximation.

The plots in Fig. 8 compare the eigenvector $v = \exp(h_{\zeta}^*)$ with the exponential of the quadratic approximation (22) given in Proposition 2.3 (iii). They are normalized so that the common maxima are equal to unity. The computations of H and $\mathcal{S}$ were based on the alternate expression for these functions that are described in Proposition A.1. The approximation is nearly perfect for the range of $|\zeta| \le 1$ (only positive values are shown due to space limitations).

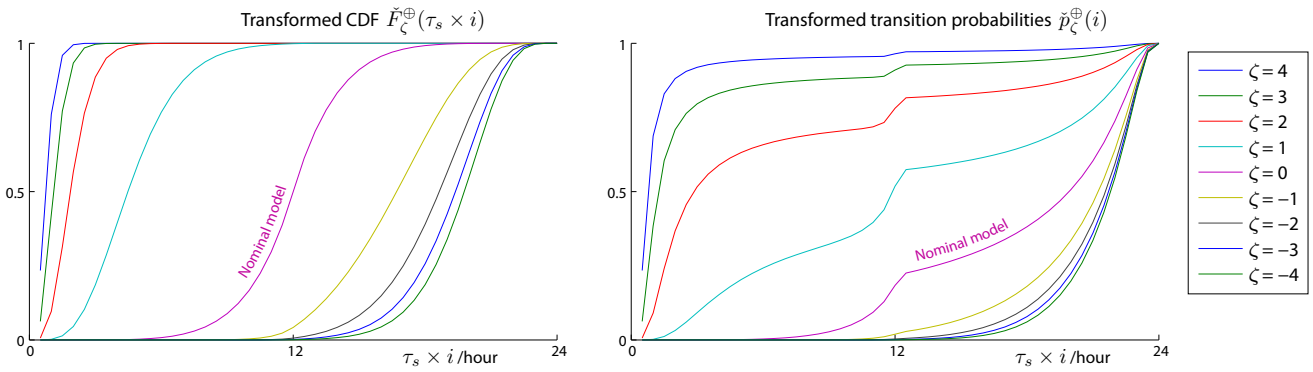

Fig. 6. Transformed probability vectors $\check{p}^{\oplus}_{\zeta}$ and corresponding discrete CDFs under $\check{P}_{\zeta}$

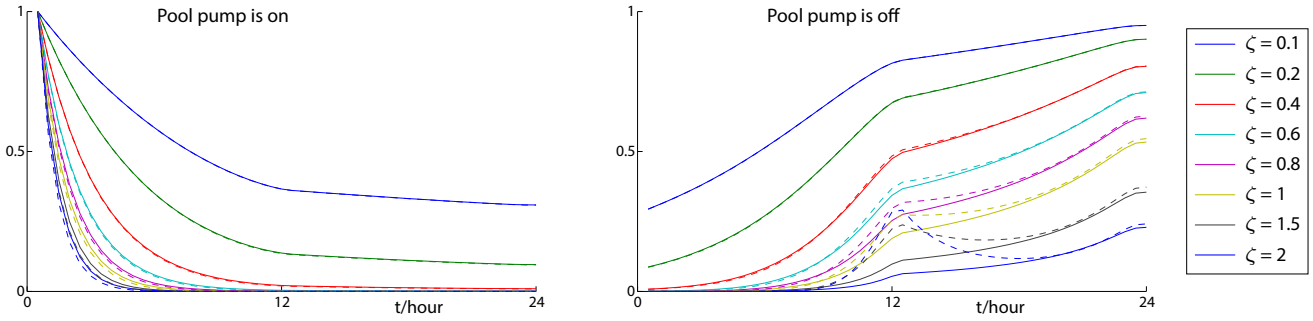

Fig. 8. Eigenvectors $v(x) = e^{h^*_{\zeta}(x)}$ (solid lines), and their approximations (dashed lines) for $\zeta > 0$. On the left $x = (\oplus, i)$ and on the right $x = (\ominus, i)$. The horizontal axis is converted to real-time using $T_s = 30$ minutes. The approximations are $\exp(C_\zeta + \zeta H(x) + \frac{1}{2}\zeta^2 \mathcal{S}(x))$, where C_ζ is independent of x.

B. Super-sampling

Recall the control architecture described at the start of Section II: at any given time, the desired power consumption/curtailment is determined by the BA. This is passed through a band-pass filter and scaled appropriately based on the proportion of ancillary service provided by the pools, and the average power consumption of pool pumps. The resulting filtered and normalized reference signal is denoted $\boldsymbol{r}$.

Super-sampling is introduced here to reduce system delay observed at the grid level. Let T_s denote the sampling interval at each pool. In this paper it has been assumed that the signal ζ_t is broadcast by the BA at time iT_s, for each $i = 0, 1, 2, \ldots$. Consider for concreteness the value $T_s = 30$ minutes. After a single broadcast, the response by the collection of loads will be nearly instantaneous – the physical delay in the system is nearly zero. Nevertheless, the control system model (26) will have a 30 minute delay, which is unacceptable. Moreover, with sampling every 30 minutes, the BA can only track signals $\boldsymbol{r}$ that are constant during the 30 minute periods between broadcast events.

To obtain a more responsive system we could place a larger burden on the loads by forcing them to check a signal from the BA more frequently, say, every minute. This would ease control at the grid level, but would also increase communication, and may not be acceptable to the consumers. An alternative is to employ "super-sampling" at the grid level.

It is convenient to model super-sampling via binning of time, so that we retain a discrete time model. We maintain the assumption that each pool checks the regulation signal at intervals of length T_s. However, the pools have no common clock. Let $m > 1$ denote a "super-sampling" parameter. At the grid-level the system is in discrete time, with sampling interval T_s/m. For example, if $T_s = 30$ minutes, then $m = 6$ corresponds to a five minute sampling interval. A pool is class i if the reference signal is observed by this load at times $nT_s + (i-1)T_s/m$, with $n \geq 0$, $1 \leq i \leq m$.

Letting y^i_t denote the fraction of pools in the ith class that are operating, the total proportion that are operating at time t is the average,

$$y_t = \frac{1}{m} \sum_{i=0}^{m-1} y^i_t$$

Let G^0 denote the discrete time transfer function using $m = 1$, which is simply the transfer function for the linear state space model (26). For general m, the transfer function from ζ to y is

$$G(z^{-1}) = z^m G^0(z^{-m}) L(z) \tag{40}$$

where L is the low pass filter,

$$L(z) = \frac{1}{m} \sum_{i=1}^{m} z^{-i} = \frac{1}{m} z^{-1} \frac{1 - z^{-m}}{1 - z^{-1}}$$

In the second representation there is a pole-zero cancellation at $z = 1$. The filter $L(z)$ has $m - 1$ zeros on the unit circle: all of the solutions to $z^m = 1$, except for the solution $z = 1$.

In real time, the delay in this LTI model is T_s/m rather than T_s. Using super-sampling we have achieved our goal of reducing delay.

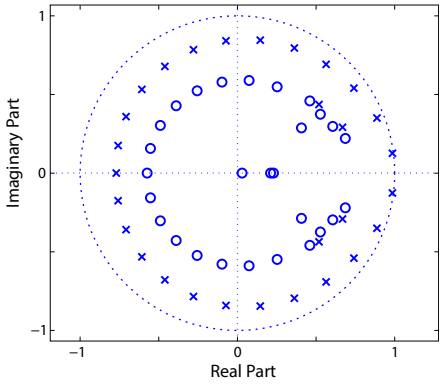

Fig. 9. Pole-zero plot for the linearized model $C[Iz - A]^{-1}B$: symmetric model with 12 hour cleaning cycle.

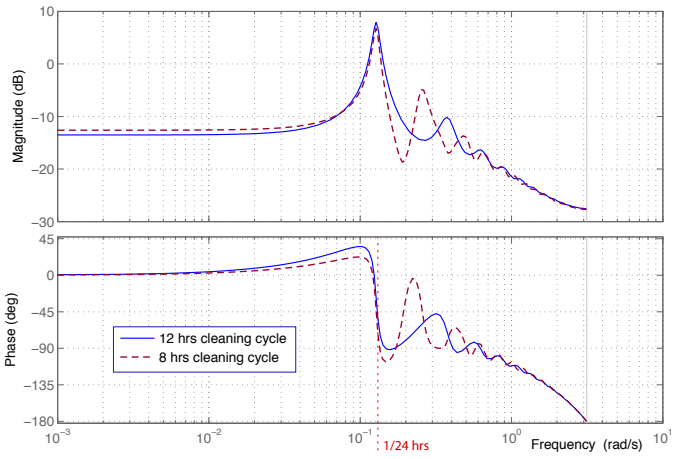

Fig. 10. Frequency response for the linearized model $C[Iz - A]^{-1}B$ in two cases: 12 and 8 hour cleaning cycles.

C. Simulation results

The numerical results described here are based on a stochastic simulation of approximately one million pools, using Matlab. This large number of pools is consistent with Florida or California [13].

The super-sampling approach was used in all experiments, with the following values of T_s and m fixed throughout: each pool checks the regulation signal every $T_s = 30$ minutes. The super-sampling parameter is $m = 6$, corresponding to 5 minutes sampling intervals at the grid level.

In simulation experiments it was assumed that the BA has perfect measurements of the total power consumption of the population of pools. We use y_t to denote the normalized power consumption, and r_t the normalized reference signal at the grid-level sampling time $t = 0, 1, 2, \dots$.

PI control was used to obtain the signal $\boldsymbol{\zeta}$: a proportional gain of 19, and integral gain of 1.4 worked well in all cases. That is, the signal $\boldsymbol{\zeta}$ was taken to be

$$\zeta_t = 19e_t + 1.4e_t^I, \quad e_t = r_t - y_t \quad \textit{and} \quad e_t^I = \sum_{k=0}^{t} e_k \tag{41}$$

This is of the form $\zeta_t = \phi_t(\mu_0, \dots, \mu_t)$, $t \geq 0$, that is required in Theorem 2.5.

Two nominal cleaning cycles were employed in the experiments, 12 and 8 hours. In each case the switching probabilities were constructed based on a pair of CDFs, using (35). For the 12-hour cleaning-cycle model, the CDF was taken to be (36) with $\gamma = 6$. An 8-hour cleaning-cycle model was obtained by using the two CDFs defined in (37) in which $\alpha = 1/3$ and $\gamma = 6$. The CDF $F^{\oplus}$ is plotted in Fig. 4.

The linearization (26) is minimum phase in each case: all zeros of $C(Iz - A)^{-1}B$ lie strictly within the unit disk in the complex plane. Fig. 9 shows the pole-zero plot for the symmetric model, and Fig. 10 shows each of the Bode plots. With the introduction of super-sampling, the resulting transfer function (40) has zeros on the unit circle.

Three categories of experiments were conducted to investigate: 1) the frequency band of regulation that the collection of pools can track, 2) the impact of cleaning cycle on the capacity of ancillary service, and 3) the performance of the algorithm when the collection of pools is heterogeneous. It was also assumed that each pool in operation consumes 1 kW. The setup for the heterogeneous model is described in Section III-C3.

In all of the experiments, $N = 999,984$ pools were used so that N is divisible by the super-sampling parameter $m = 6$.

1) The need for filtering: The goal here is to find an appropriate frequency band of regulation that pool pumps can provide. The symmetric model based on a 12-hour cleaning cycle per day was used in simulations.

Suppose that the BPA signal is used to define the reference $\boldsymbol{r}$ without any pre-filtering, but scaled to a comparable magnitude with the low-pass filtered signal shown in Fig. 1. To ease comparison, only the first 48 hours of output from the simulation is shown. In simulations we find that there is noticeable tracking error using the PI control (41). A typical result from simulations is shown on the left hand side of Fig. 11. If the reference signal $\boldsymbol{r}$ is chosen to be the low-pass filtered signal, then tracking performance is nearly perfect, as shown on the right hand side of Fig. 11.

We conclude that one million pools can provide ancillary service in this low frequency band, with negligible tracking error.

The filtered reference signal was used in all subsequent experiments.

2) Cleaning cycle and capacity: It was found that one million pools can provide far more regulation than the $\pm$ 200 MW required at BPA during the week corresponding to Fig. 1. More experiments were conducted in which the filtered signal was scaled to investigate the limits of regulation from a population of one million pools.

We summarize results obtained from two sets of experiments conducted in two scenarios. In the first, we used the symmetric model with cleaning cycle of 12 hours per day. The second scenario was based on the asymmetric model with 8-hour cleaning cycle.

The average proportion of time that a pool is on will be approximately $1/2$ in Scenario 1, and $1/3$ in Scenario 2. Consequently, the class of regulation signals that can be tracked is not symmetric in Scenario 2: the population of pools has more potential for increasing rather than decreasing power consumption.

To attempt to quantify this effect, define *potential capacity* as the upper and lower limits of power deviation, subject

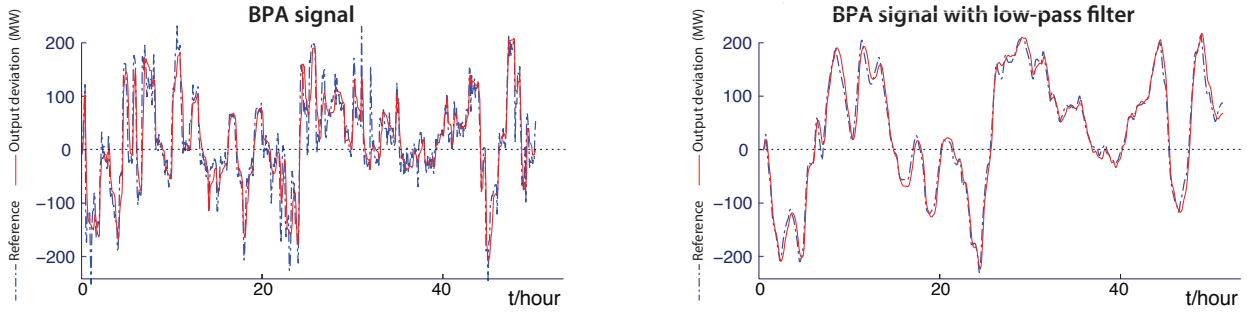

Fig. 11. Tracking performance using PI control with one million pools. Performance is improved when the BPA signal is passed through a low-pass filter.

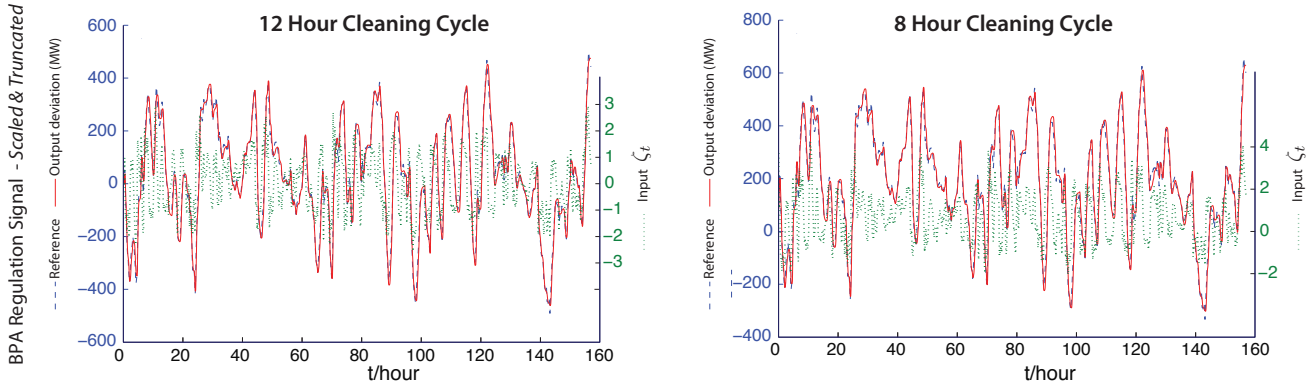

Fig. 12. Closed loop simulation in two scenarios.

to the constraint that tracking performance does not degrade significantly, denoted $\{+\text{Demand}, -\text{Supply}\}$. In simulations we observe a phase transition: the performance is nearly perfect until the regulation signal reaches upper or lower limits. Moreover, these limits nearly coincide with values obtained from the following heuristic. Let $\pi_0^{\oplus}$ denote the fraction of pool pumps that are operating in nominal steady-state,

$$\pi_0^{\oplus} = \sum_i \pi_0(\oplus, i)$$

where π_0 is invariant for P_0. The heuristic is then given by $\{+\text{Demand}, -\text{Supply}\} \approx \{(1 - \pi_0^{\oplus}) \times N, -\pi_0^{\oplus} \times N\}$ kW. In Scenario 1 this gives the approximation $\{+500MW, -500MW\}$, and $\{+659MW, -341MW\}$ in Scenario 2.

Results from two experiments are shown in Fig. 12. The low-pass filtered signal shown in Fig. 1 was scaled in magnitude to match its potential capacity. In addition, a DC offset was used in the experiments using the 8 hour cleaning cycle — this allowed for greater overall capacity from these loads. The provision of the DC component of power would be from traditional generation resources, and not the loads. The tracking performance is remarkable. In particular, it is surprising that a ± 400 MW signal can be tracked, given that the average power consumption of the pools is 500 MW in Scenario 1.

Subplots (a) and (b) in Fig. 13 show what happens when the reference signal exceeds capacity. Two sources of error are evident in these plots. First, the power deviation saturates when all of the $N \approx 10^6$ pools are turned off, or all are turned on. Secondly, large tracking errors are observed immediately after saturation. This is a consequence of memory in the PI controller – what is known as *integrator windup*. To solve this problem, the BA should truncate the regulation signal so that it does not exceed the values $\{+\text{Demand}, -\text{Supply}\}$. Subplots (c) and (d) in Fig. 13 use the same regulation signal used in (a), (b), but truncated to meet these capacity constraints. Once again, the tracking is nearly perfect.

3) Heterogeneous population: Consider a population of pools in which the cleaning cycle and power consumption vary from pool to pool. The control architecture remains the same: the command $\boldsymbol{\zeta}$ is defined using the PI control law (41), where $\boldsymbol{y}$ is again the normalized power consumption of the population.

Results from a special case are summarized here, in which the population of pools is the union of four homogeneous classes. Each class consists of $N/4$ pools that are differentiated by cleaning cycle and power consumption: the cleaning cycle is either 12 or 8 hours per day, and power consumption of a pool pump in one class is either 1 kW or 2 kW. Hence there are $N \approx 10^6$ pools in total, with peak power consumption of approximately 1.5 GW. By considering each of the four classes separately, the heuristic gives $\{+\text{Demand}, -\text{Supply}\} = \{+869MW, -631MW\}$. The potential capacity observed in simulation experiments closely matched this approximation.

This model admits a linearization in which the transfer function G from $\boldsymbol{\zeta}$ to $\boldsymbol{y}$ is the average of the transfer functions of the four classes of pools, where each transfer function has the same form as in the homogeneous case. Letting G^k denote the transfer function obtained with cleaning cycle k and 1 kW

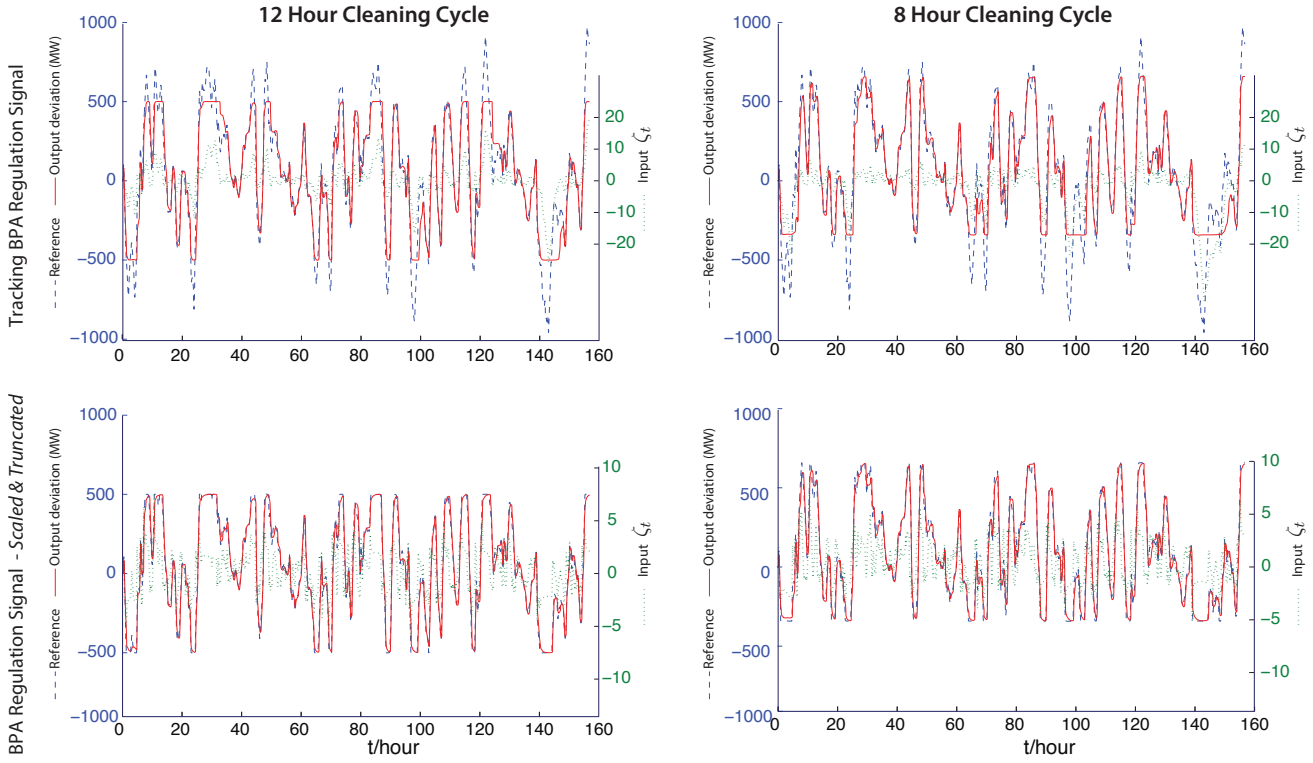

Fig. 13. The impact of exceeding capacity

power consumption, the overall transfer function is given by,

$$G = \tfrac{1}{4}\Big(G^8 + 2G^8 + G^{12} + 2G^{12}\Big) = \tfrac{3}{4}\Big(G^8 + G^{12}\Big)$$

The first plot in Fig. 14 shows that the tracking performance is again nearly perfect. The response of each class of pools in the population is more complex. Shown on the right hand side of Fig. 14 is the power consumption from two of the four classes: 12 and 8 hour cleaning cycle, each with 1 kW maximal power consumption. The plots of the outputs for the other two classes (with 2 kW power consumption) are nearly the same as those shown in Fig. 14, but scaled by a factor of 2.

The pools with 12-hour cleaning cycle provide a larger contribution to the reference signal than the pools with 8-hour cleaning cycle. The two classes of pools also contribute very differently in behavior. At times, the deviations in power consumption are of different signs. This 'lack of cooperation' is reduced when the reference signal is scaled upwards: When the reference signal is near capacity, the power deviations of one class is nearly a constant multiple of the other.

IV. Conclusions

The simplicity of the MDP solution, and the remarkable accuracy of the LTI approximation for the mean-field model makes this approach appealing for this and related applications.

We hope it is clear to the reader that the application of these techniques go beyond pool pumps. In the context of a power grid, a large collection of on/off loads can provide ancillary service at high capacity and over a large frequency range using a randomized control architecture of the form described in this paper. In many parts of the world, more valuable than pools are the chillers in heating and ventilation systems. These loads are nearly as flexible as pools, and consume a great deal of power. Harnessing ancillary service from chillers requires greater attention to dynamics and constraints at the load. This is a topic of current research.

There are several issues that have not been addressed here:

(i) The construction and analysis of randomized policies deserves further consideration. We are currently considering settings for which some randomness is exogenous in the nominal model. For example, in the case of a heating and ventilation system, the weather and building occupancy are sources of exogenous randomness. We are also working to understand why the linearization should be minimum phase – preliminary work is contained in [35].

(ii) We do not fully understand the potential cost to consumers in terms of energy, or risk in terms of rare events in which the pool is under- or over-cleaned. It is likely that hard constraints on performance can be put in place without impacting the analysis: Preliminary results are contained in the sequel [15], along with methods to approximate the distribution of risk.

(iii) Does the grid operator need to know the real-time power consumption of the population of pools? The grid frequency passed through a band-pass filter could serve as a surrogate for the measurement y_t assumed in this paper.

Alternatively, it may be valuable to have *two* mea-

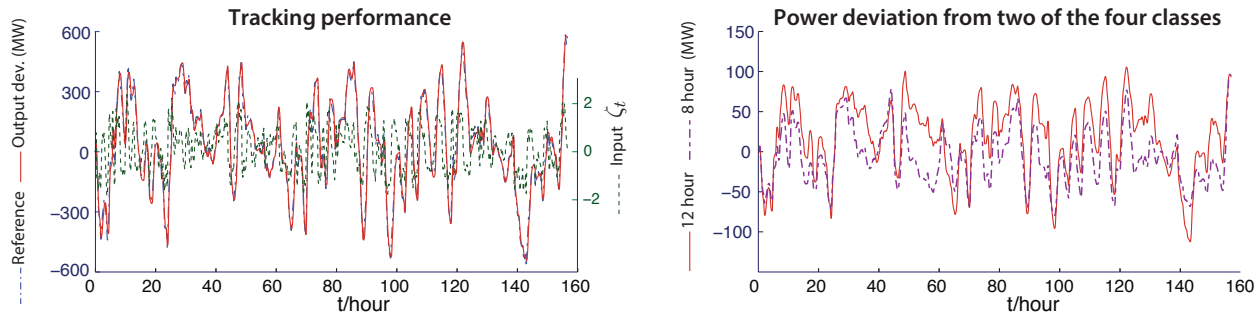

Fig. 14. Tracking performance in heterogeneous case, and power deviation from two of the four classes (with 1 kW maximal power consumption).

surements at each load: the BA command, and *local* frequency.

(iv) How can we engage consumers? FERC order 755 that demands "mileage payments" for ancillary services may provide a mechanism for incentivizing consumers today. It is envisioned that these payments will be part of a bilateral contract between the consumer and a BA or aggregator. The formulation of contracts with customers requires a better understanding of the value of ancillary service, as well as consumer preferences.

REFERENCES

[1] "FPL On Call Saving Program," Online, http://tinyurl.com/FPL-OnCall.

[2] J. MacDonald, P. Cappers, D. S. Callaway, and S. Kiliccote, "Demand response providing ancillary services a comparison of opportunities and challenges in the U.S. wholesale markets," in *Grid-Interop*, Irving, TX, December 2012.

[3] "BPA balancing authority," Online, http://tinyurl.com/BPAgenload, http://tinyurl.com/BPAbalancing.

[4] H. Hao, Y. Lin, A. Kowli, P. Barooah, and S. Meyn, "Ancillary service to the grid through control of fans in commercial building HVAC systems," *IEEE Trans. on Smart Grid*, vol. 5, no. 4, pp. 2066–2074, July 2014.

[5] Y. Lin, P. Barooah, S. Meyn, and T. Middelkoop, "Experimental evaluation of frequency regulation from commercial building HVAC systems," *IEEE Trans. on Smart Grid*, vol. [DOI : 10.1109/TSG.2014.2381596], no. 99, pp. 1–1, 2015.

[6] H. Hao, T. Middelkoop, P. Barooah, and S. Meyn, "How demand response from commercial buildings will provide the regulation needs of the grid," in *50th Allerton Conference on Communication, Control, and Computing*, 2012, pp. 1908–1913.

[7] Y. Lin, P. Barooah, and S. Meyn, "Low-frequency power-grid ancillary services from commercial building HVAC systems," in *IEEE Conference on Smart Grid Communications (SmartGridComm)*, Oct 2013, pp. 169–174.

[8] D. Todd, B. Helms, M. Caufield, M. Starke, B. Kirby, and J. Kueck, "Providing reliability services through demand response: A preliminary evaluation of the demand response capabilities of Alcoa Inc." LBNL and Alcoa, Tech. Rep., January 2009, report no. ORNL/TM-2008/233.

[9] R. Srikant, *The mathematics of Internet congestion control*, ser. Systems & Control: Foundations & Applications. Boston, MA: Birkhäuser Boston Inc., 2004.

[10] S. Floyd and V. Jacobson, "Random early detection gateways for congestion avoidance," *IEEE/ACM Trans. Netw.*, vol. 1, no. 4, pp. 397–413, 1993.

[11] E. Todorov, "Linearly-solvable Markov decision problems," in *Advances in Neural Information Processing Systems 19*, B. Schölkopf, J. Platt, and T. Hoffman, Eds. Cambridge, MA: MIT Press, 2007, pp. 1369–1376.

[12] I. Kontoyiannis and S. P. Meyn, "Large deviations asymptotics and the spectral theory of multiplicatively regular Markov processes," *Electron. J. Probab.*, vol. 10, no. 3, pp. 61–123 (electronic), 2005.

[13] C. S. B. U. Design & Engineering Services, "Pool pump demand response potential: Demand and run-time monitored data. DR 07.01 Report. Prepared by: Design & Engineering Services, Customer Service Business Unit, Southern California Edison," Online, www.etcc-ca.com/images/stories/pdf/ETCC_Report_473.pdf, pp. 12–34, June 2008.

[14] K. Hall and M. Lo, "Survey of residential swimming pools assessed by Florida county property appraisers, Summer 2006," Florida Department of Health, Tech. Rep., 2006.

[15] Y. Chen, A. Bušić, and S. Meyn, "Individual risk in mean-field control models for decentralized control, with application to automated demand response," 2014, 53rd IEEE Conf. on Decision and Control (Invited).

[16] J. Mathieu, S. Koch, and D. Callaway, "State estimation and control of electric loads to manage real-time energy imbalance," *IEEE Trans. Power Systems*, vol. 28, no. 1, pp. 430–440, 2013.

[17] B. Biegel, L. Hansen, P. Andersen, and J. Stoustrup, "Primary control by ON/OFF demand-side devices," *IEEE Trans. on Smart Grid*, vol. 4, no. 4, pp. 2061–2071, Dec 2013.

[18] B. Sanandaji, H. Hao, and K. Poolla, "Fast regulation service provision via aggregation of thermostatically controlled loads," in *47th Hawaii International Conference on System Sciences (HICSS)*, Jan 2014, pp. 2388–2397.

[19] Z. Ma, D. Callaway, and I. Hiskens, "Decentralized charging control for large populations of plug-in electric vehicles: Application of the Nash certainty equivalence principle," in *IEEE International Conf. on Control Applications (CCA)*, 2010, pp. 191–195.

[20] R. Couillet, S. Perlaza, H. Tembine, and M. Debbah, "Electrical vehicles in the smart grid: A mean field game analysis," *IEEE J. Selected Areas in Comm.*, vol. 30, no. 6, pp. 1086–1096, 2012.

[21] M. Huang, P. E. Caines, and R. P. Malhame, "Large-population cost-coupled LQG problems with nonuniform agents: Individual-mass behavior and decentralized ε-Nash equilibria," *IEEE Trans. Automat. Control*, vol. 52, no. 9, pp. 1560–1571, 2007.

[22] V. Borkar and R. Sundaresan, "Asymptotics of the invariant measure in mean field models with jumps," *Stochastic Systems*, vol. 2, no. 2, pp. 322–380, 2012.

[23] N. Gast, B. Gaujal, and J.-Y. Le Boudec, "Mean field for Markov decision processes: From discrete to continuous optimization," *IEEE Trans. Automat. Control*, vol. 57, no. 9, pp. 2266–2280, 2012.

[24] P. Harsha, M. Sharma, R. Natarajan, and S. Ghosh, "A framework for the analysis of probabilistic demand response schemes," *IEEE Trans. on Smart Grid*, vol. 4, no. 4, pp. 2274–2284, 2013.

[25] K. Christakou, D.-C. Tomozei, J.-Y. Le Boudec, and M. Paolone, "GECN: primary voltage control for active distribution networks via real-time demand-response," *IEEE Trans. on Smart Grid*, vol. 5, no. 2, pp. 622–631, March 2014.

[26] J. Unnikrishnan, D. Huang, S. P. Meyn, A. Surana, and V. V. Veeravalli, "Universal and composite hypothesis testing via mismatched divergence," *IEEE Trans. Inform. Theory*, vol. 57, no. 3, pp. 1587 – 1603, 2011.

[27] A. Dembo and O. Zeitouni, *Large Deviations Techniques And Applications*, 2nd ed. New York: Springer-Verlag, 1998.

[28] S. Meyn, P. Barooah, A. Bušić, and J. Ehren, "Ancillary service to the grid from deferrable loads: The case for intelligent pool pumps in Florida," in *Proceedings of the 52nd IEEE Conf. on Decision and Control*, Dec 2013, pp. 6946–6953.

[29] S. P. Meyn and R. L. Tweedie, *Markov chains and stochastic stability*, 2nd ed. Cambridge: Cambridge University Press, 2009, published in the Cambridge Mathematical Library. 1993 edition online.

[30] E. Seneta, *Non-Negative Matrices and Markov Chains*, 2nd ed. New York, NY: Springer, 1981.

[31] E. Nummelin, *General Irreducible Markov Chains and Nonnegative Operators*. Cambridge: Cambridge University Press, 1984.

[32] S. P. Meyn, *Control Techniques for Complex Networks*. Cambridge University Press, 2007, pre-publication edition available online.

[33] V. S. Borkar, "Convex analytic methods in Markov decision processes," in *Handbook of Markov decision processes*, ser. Internat. Ser. Oper. Res. Management Sci. Boston, MA: Kluwer Acad. Publ., 2002, vol. 40, pp. 347–375.

[34] C. McDiarmid, "Concentration," in *Probabilistic methods for algorithmic discrete mathematics*, ser. Algorithms Combin., M. Habib, C. McDiarmid, J. Ramirez-Alfonsin, and B. Reed, Eds. Berlin: Springer, 1998, vol. 16, pp. 195–248.

[35] A. Bušić and S. Meyn, "Passive dynamics in mean field control," *CoRR*, vol. abs/1402.4618, 2014, 53rd IEEE Conf. on Decision and Control (Invited). [Online]. Available: http://arxiv.org/abs/1402.4618

APPENDIX

A. Controlled transition matrix: Proof of Proposition 2.2.

The dependency of η^*, $h = \log(v)$, and λ on ζ will be suppressed to simplify notation in the proof of Proposition 2.2 that follows.

The existence of a unique maximal eigenvalue and a positive eigenvector is a consequence of the Perron-Frobenious Theorem [30], [31]. Recent results on this and associated multiplicative ergodic theory are contained in [12], from which the identity $\Lambda := \log(\lambda) = \eta^*_\zeta$ is established (see [12, Theorem 1.2]).

The bounds in (11) imply a rate of convergence of the finite horizon cost using $\check{P}$ to its infinite-horizon limit, which in particular implies that $\Lambda := \log(\lambda) = \eta^*_\zeta$. To complete the proof of Proposition 2.2 it remains to establish this pair of bounds.

We begin with the second bound in (11). Let $\check{p}_T$ denote the probability on strings on X^T induced by $\check{P}$, with initial condition x_0 given, and let x_1^T denote the string $(x_1, \dots, x_T)$. We have,

$$\check{p}_T(x_1^T) = \frac{v(x_T)}{v(x_1)} \exp\big(\zeta \sum_{t=1}^T \mathcal{U}(x_t) - T\Lambda\big) p_0(x_1^T)$$

and since $\check{p}_T$ is a probability mass function,

$$\begin{aligned} 1 &= \sum_{x_1,\dots,x_T} \check{p}_T(x_1^T) \\ &= \sum_{x_1,\dots,x_T} \frac{v(x_T)}{v(x_1)} \exp\Big(\zeta \sum_{t=1}^T \mathcal{U}(x_t) - T\Lambda\Big) p_0(x_1^T) \end{aligned}$$

which gives,

$$T\Lambda = \log\Big\{ \mathsf{E}\Big[\frac{v(X_T)}{v(X_1)} \exp\Big(\zeta \sum_{t=1}^T \mathcal{U}(X_t)\Big)\Big]\Big\}.$$

The bound on $|T\Lambda - \mathcal{W}_T(p_T^*)|$ follows from this identity combined with Proposition 2.1 (which establishes $\mathcal{W}_T(p_T^*) = \Lambda_T(\zeta)$).

Substitution of $\check{p}_T$ into the definition of $\mathcal{W}_T$ gives,

$$\mathcal{W}_T(\check{p}_T) = -\mathsf{E}_p\Big[\log(v(X(T)) - \log(v(X(1))\Big] + T\Lambda$$

This combined with the second bound in (11) gives the desired upper bound on $\mathcal{W}_T(p_T^*) - \mathcal{W}_T(\check{p}_T)$. ☐

B. Computation

The specification of the transition matrix $\check{P}_\zeta$ in (9) is based on the optimal average cost η^*_ζ that is defined in (4), the relative value function h^*_ζ introduced in (10), and the nominal transition matrix P_0.

Approximations of η^*_ζ and h^*_ζ are based on Poisson's equation. In general, we say that g *is the solution to Poisson's equation with forcing function* f if the following equation holds:

$$g - P_0 g = f \tag{42}$$

For this finite state space Markov chain, it follows from invariance of π_0 that $\pi_0(f) = \sum_x \pi_0(x) f(x) = 0$.

We show here that the second order term $\mathcal{S}$ defined in (18) can be expressed as a solution to a certain Poisson equation, and explain how to compute solutions.

1) Poisson's equation: This is a finite state Markov chain, so Perron-Frobenious theory is very simple and attractive [12], [30], [31]. Let $s\colon \mathsf{X} \to \mathbb{R}_+$ be a function (not identically zero), and ν a probability mass function such that the *minorization condition* holds,

$$P_0(x, y) \ge s(x)\nu(y), \qquad x, y \in \mathsf{X}$$

This is written $P_0 \ge s \otimes \nu$. We will take $s(x) = \mathbb{I}\{x = \boldsymbol{\alpha}\}$ and $\nu(y) = P_0(\boldsymbol{\alpha}, y)$, so that for all y,

$$\overline{P}(x, y) := P_0(x, y) - s(x)\nu(y) = \begin{cases} 0 & x = \alpha \\ P_0(x, y) & x \neq \alpha \end{cases}$$

The inverse $Z = [I - \overline{P}]^{-1}$ is called the potential matrix [31].

The invariant probability mass function π_0 can be expressed in terms of a matrix inverse. We first use the implication,

$$\pi_0 P_0 = \pi_0 \Longrightarrow \pi_0(P_0 - s \otimes \nu) = \pi_0 - \delta\nu$$

where $\delta = \sum_x \pi_0(x) s(x)$ is a constant. We then invert,

$$\pi_0 = \delta\nu[I - (P_0 - s \otimes \nu)]^{-1} = \delta\nu Z$$

The measure $\mu = \nu Z$ is an unnormalized invariant measure. Normalization gives the invariant probability measure,

$$\pi_0(x) = \mu(x)/[\sum_y \mu(y)], \qquad x \in \mathsf{X}.$$

A similar computation is used to solve Poisson's equation. Assume that $\nu(H) = \sum \nu(x) H(x) = 0$. This is without loss of generality. Under this assumption,

$$\widetilde{\mathcal{U}} + P_0 H = H \Longrightarrow \widetilde{\mathcal{U}} + (P_0 - s \otimes \nu) H = H$$

which gives $H = Z\widetilde{\mathcal{U}}$.

2) Second-order approximation: Let h'_ζ and h''_ζ denote the first and second derivatives of h^*_ζ with respect to the argument ζ. Each of these are real-valued functions on X. The Taylor series approximation (22) in Proposition 2.3 implies that

$$h'_\zeta\Big|_{\zeta=0} = H \quad \textit{and} \quad h''_\zeta\Big|_{\zeta=0} = \mathcal{S}\,.$$

Here we obtain representations of these functions that are convenient for computation.

We show in Proposition A.1 that $\mathcal{S}$ solves a certain Poisson equation, that can be solved through elementary matrix algebra. The representation for h_ζ'' in Proposition A.1 appears to be new.

The derivations are most easily obtained using the *nonlinear generator*, defined for any function $g\colon \mathsf{X} \to \mathbb{R}$ via,

$$\mathcal{H}(g) := \mathcal{P}(g) - g,$$

where $\mathcal{P}(g)$ denotes the function,

$$\mathcal{P}(g)\Big|_x := \log(Pe^g)\Big|_x = \log\Big(\sum_y P(x,y)e^{g(y)}\Big), \qquad x \in \mathsf{X}$$

Using this notation, the eigenvector equation can be expressed in a form similar to Poisson's equation,

$$h_\zeta^* - \mathcal{P}(h_\zeta^*) = z\mathcal{U} - \eta_\zeta^* \tag{43}$$

in which $z\mathcal{U} - \eta_\zeta^*$ plays the role of a forcing function, similar to (42). The similarity between (42) and (43) is why h_ζ^* is called the solution to the *multiplicative Poisson equation* in [12].

We also require a nonlinear operator that defines one-step variance: For any function $g\colon \mathsf{X} \to \mathbb{R}$,

$$\mathcal{V}(g)\Big|_x := \sum_y P_0(x,y)g^2(y) - \Big[\sum_y P_0(x,y)g(y)\Big]^2$$

That is, $\mathcal{V}(g) = Pg^2 - [Pg]^2$.

Proposition A.1: The functions h_ζ' and h_ζ'' solve the following Poisson equations:

$$\mathcal{U} + \check{P}_\zeta h_\zeta' = h_\zeta' + \Lambda_\zeta' \tag{44}$$
$$\mathcal{V}(h_\zeta') + \check{P}_\zeta h_\zeta'' = h_\zeta'' + \Lambda_\zeta'' \tag{45}$$

where $\Lambda_\zeta = \log(\lambda_\zeta) = \eta_\zeta^*$. The derivatives also satisfy the boundary conditions,

$$h_\zeta'(\boldsymbol{\alpha}) = h_\zeta''(\boldsymbol{\alpha}) = 0.$$

In particular, with $\zeta = 0$ we obtain,

$$\mathcal{U} + P_0 H = H + \eta_0$$
$$\mathcal{V}(H) + P_0 \mathcal{S} = \mathcal{S} + \kappa^2$$

□

Proof: The boundary conditions hold because $h_\zeta^*(\boldsymbol{\alpha}) = \log(v(\boldsymbol{\alpha})) = 0$ for all ζ. This is by construction — see (13) and (12).

The remaining results are obtained by differentiating each side of (43). The first derivative of $\mathcal{P}(h_\zeta^*)$ is obtained from simple calculus:

$$\frac{d}{d\zeta}\mathcal{P}(h_\zeta^*) = \frac{d}{d\zeta}\log(Pe^{h_\zeta^*}) = \frac{1}{Pe^{h_\zeta^*}}P\{e^{h_\zeta^*}h_\zeta'\} = \check{P}_\zeta h_\zeta' \tag{46}$$

On differentiating each side of (43) we thus obtain (44).

For the second derivative of h_ζ^* we require the second derivative of $\mathcal{P}(h_\zeta^*)$. A representation will follow from the product rule, using (46):

$$\frac{d^2}{d\zeta^2}\mathcal{P}(h_\zeta^*) = \check{P}_\zeta h_\zeta'' + \check{P}_\zeta' h_\zeta' \tag{47}$$

To obtain an expression for the matrix $\check{P}_\zeta'$, observe that for any $x, y \in \mathsf{X}$ for which $P_0(x,y) > 0$,

$$\begin{aligned}\frac{d}{d\zeta}\log\big(\check{P}_\zeta(x,y)\big) &= \frac{d}{d\zeta}\log\big(P(x,y)e^{h_\zeta^*(y)}/Pe^{h_\zeta^*}(x)\big)\\ &= h_\zeta'(y) - \frac{d}{d\zeta}\mathcal{P}(h_\zeta^*)\Big|_x = h_\zeta'(y) - \check{P}_\zeta h_\zeta'(x)\end{aligned}$$

where the final equality follows from (46). This gives,

$$\frac{d}{d\zeta}\check{P}_\zeta(x,y) = \check{P}_\zeta(x,y)[h_\zeta'(y) - \check{P}_\zeta h_\zeta'(x)], \qquad x, y \in \mathsf{X}.$$

Substituting this into (47) gives,

$$\begin{aligned}\frac{d^2}{d\zeta^2}\mathcal{P}(h_\zeta^*)\Big|_x &= \check{P}_\zeta h_\zeta''(x) + \check{P}_\zeta' h_\zeta'(x)\\ &= \check{P}_\zeta h_\zeta''(x) + \sum_y \check{P}_\zeta(x,y)[h_\zeta'(y) - \check{P}_\zeta h_\zeta'(x)]h_\zeta'(y)\end{aligned}$$

which simplifies to,

$$\frac{d^2}{d\zeta^2}\mathcal{P}(h_\zeta^*) = \check{P}_\zeta h_\zeta'' + \mathcal{V}(h_\zeta')$$

Differentiating each side of (43) twice thus gives (45). □

Sean P. Meyn (S'85, M'87, SM'95, F'02) received the B.A. degree in Mathematics Summa Cum Laude from UCLA in 1982, and the PhD degree in Electrical Engineering from McGill University in 1987 (with Prof. P. Caines). He held a two year postdoctoral fellowship at the Australian National University in Canberra, and was a professor at the University of Illinois from 1989-2011. Since January, 2012 he has been a professor and has held the Robert C. Pittman Eminent Scholar Chair in Electrical and Computer Engineering at the University of Florida. He is coauthor with Richard Tweedie of the monograph Markov Chains and Stochastic Stability, Springer-Verlag, London, and received jointly with Tweedie the 1994 ORSA/TIMS Best Publication In Applied Probability Award. His research interests include stochastic processes, optimization, complex networks, and information theory, with applications to smarter cities and smarter grids.

Prabir Barooah is an Associate Professor of Mechanical and Aerospace Engineering at the University of Florida, where he has been since 2007. He received the Ph.D. degree in Electrical and Computer Engineering in 2007 from the University of California, Santa Barbara. From 1999 to 2002 he was a research engineer at United Technologies Research Center, East Hartford, CT. He received the M. S. degree in Mechanical Engineering from the University of Delaware in 1999 and the B. Tech. degree in Mechanical Engineering from the Indian Institute of Technology, Kanpur, in 1996. Dr. Barooah is the winner of the ASEE-SE (American Society of Engineering Education, South East Section) outstanding researcher award (2012), NSF CAREER award (2010), General Chairs' Recognition Award for Interactive papers at the 48th IEEE Conference on Decision and Control (2009), best paper award at the 2nd Int. Conf. on Intelligent Sensing and Information Processing (2005), and NASA group achievement award (2003).

Ana Bušić is a Research Scientist at Inria Paris – Rocquencourt, and a member of the Computer Science Department at Ecole Normale Supérieure, Paris, France. She received a M.S. degree in Mathematics in 2003, and a Ph.D. degree in Computer Science in 2007, both from the University of Versailles. She was a post-doctoral fellow at Inria Grenoble – Rhône-Alpes and at University Paris Diderot-Paris 7. She joined Inria in 2009. She is a member of the Laboratory of Information, Networking and Communication Sciences, a joint lab between Alcatel-Lucent, Inria, Institut Mines-Télécom, UPMC Sorbonne Universities, and SystemX. Her research interests include stochastic modeling, simulation, performance evaluation and optimization, with applications to communication networks and energy systems.

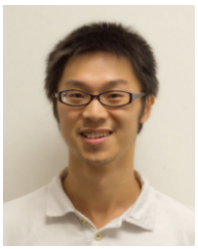

Yue Chen (S' 14) received the B.E. degree in electronic and information engineering from Harbin Engineering University, Harbin, China, in 2008, the M.E. degree in electrical engineering from University of Detroit Mercy, Detroit, USA, in 2010, the M.S. degree in Electrical and Computer Engineering in 2012 from University of Florida, Gainesville, USA. He is currently working toward the Ph.D. degree in electrical and computer engineering at University of Florida.

Jordan Ehren (S' 14) is an undergraduate student at the University of Florida, majoring in Electrical Engineering, and set to graduate in 2016. He has worked in the Laboratory for Cognition and Control in Complex systems since its creation in 2012, supported in part through an NSF REU award. His research has also been supported through the UF University Scholars program. His interests include renewable energy, energy storage and intelligent power grids.